Journal of Materials Chemistry A

Accepted Manuscript

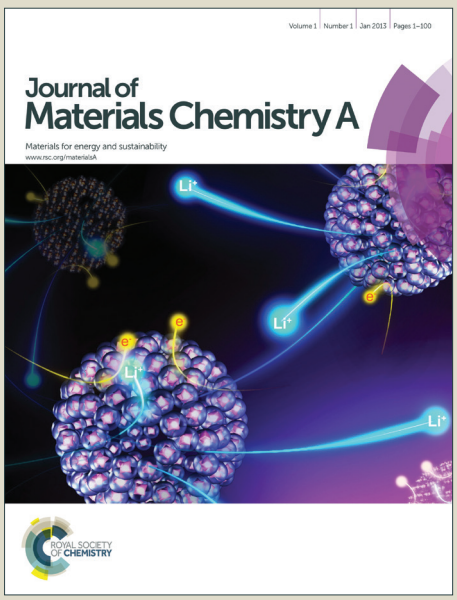

ROYAL SOCIETY OF CHEMISTRY

www.rsc.org/materialsA

Journal of Materials Chemistry A RSCPublishing

ARTICLE

Facile Synthesis of Three-Dimensional Mn_3O_4 Hierarchical Microstructures and Their Application in the Degradation of Methylene Blue

Cite this: DOI: 10.1039/x0xx00000x

Yuli Wang,[a] Ling Zhu,[a] Xing Yang,[b] Erlei Shao,[b] Xiaoyong Deng,[*b] Ning Liu,[a] Minghong Wu[*a]

Received 00th January 2014,
Accepted 00th January 2014

DOI: 10.1039/x0xx00000x

www.rsc.org/

A simple and effective route has been developed to synthesize three-dimensional (3D) Mn_3O_4 hierarchical architecture, which shows flower-like morphology and is composed of Mn_3O_4 nanosheets. Two experimental parameters, the hydrothermal temperature and NaOH addition speed, were revealed to have the critical effects on the formation of morphology. Furthermore, these Mn_3O_4 materials were successfully applied to degrade the organic pollutants in water. Compared with Mn_3O_4 nanoparticles and nanorods, 3D flower-like Mn_3O_4 nanostructures are found to the most heavily enhance the MB degradation efficiency of the UV/H_2O_2 advanced oxidation process (AOP), which comes from their high BET surface area and good absorption ability.

Introduction

Hausmannite (Mn_3O_4), due to its special optical, electrical and magnetic properties,[1] has attracted considerable interest and been widely used in a large number of applications, including active catalysts,[2] electrochemical reactions and batteries[1a,1c,3] and soft magnetic materials.[4] Different from bulk materials, the micro/nanosized transition-metal oxides usually show size-, structure- and morphology-dependent characteristics and possess a variety of special physical, chemical and functional properties.[5] Therefore, various morphologies of Mn_3O_4 with different size have been synthesized by different methods.

Among them, zero-dimensional (0D) Mn_3O_4 nanoparticles are the most heavily investigated. Many methods have been developed, such as hydrothermal method,[2e,6] sol-gel process,[7] thermal decomposition,[8] two-phase hydrolysis approach[9] and so on, to synthesize spherical, cubic, octahedral or rodlike Mn_3O_4 nanoparticles. As to one dimensional (1D) Mn_3O_4 nanomaterials, Wang et al. firstly synthesized Mn_3O_4 nanowires with diameter of 40-80 nm and length of up to 150 um via high temperature growth in 2002.[10] After that, many other groups have developed a range of methods to produce Mn_3O_4 nanowires[11] and nanotubes[12]. In 2009 and 2010, Hyeon's group[1b] and Li's group[13] respectively reported two versatile synthetic strategies for the controllable preparation of Mn_3O_4 with different sizes and shapes, from 0D nanocrystals, nanorods and nanoplates, to 1D nanowires. Our group has also indicated that different Mn_3O_4 nanomorphologies, including nanoparticles, nanorods and nanofractals, could be shaped by just controlling the dripping speed of NaOH solutions.[14] As to two dimensional (2D) Mn_3O_4 nanomaterials, very few groups, less than five reports, have successfully synthesized nanosheets or nanoplates due to the natural non-layered Mn_3O_4 structure. For instance, Mn_3O_4 nanosheets have been produced from aqueous chemical reaction,[15] and the layered bulk material by a procedure of exfoliation.[16] Very recently, Chen et al. prepared mesoporous Mn_3O_4 nanoplates on the graphene under room temperature, with a size of about 100 nm and a thickness of 15 nm.[17] In all, preparation of Mn_3O_4 nanomaterials with a controlled size and morphology has drawn tremendous attention.

Recently, three-dimensional (3D) hierarchical nanostructures assembled by nanoscaled building blocks such as nanoparticles, nanorods, nanosheets and others, have been attracting more and more attention.[18] More than 2000 publications have been published in this area since 2012. The hierarchical nanostructures not only combine the properties of nanoscaled building blocks, but also will show unique features different from those of the mono-morphological structures.[19] In fact, the controlled formation of 3D complex functional architecture is the key in developing more sophisticated nanostructure and is expected to offer great opportunities for the fabrication of new nanostructures and for exploring their novel properties.[20] Thus, it is very important to develop facile routes to prepare 3D hierarchical nanostructures. However, dimensionality control and assembly of complex nanostructures remain the most intricate, which is still one of challenging areas in the study of micro/nanomaterials.[21] As an important functional metal oxide material, 3D Mn_3O_4 micro/nanomaterials have been prepared by few groups.[13,22,23] Pan's group has successfully synthesized Mn_3O_4 nanostructures with three-dimensionally intercrossing nanowires;[22b] Li et al. adopted the ultrasonication strategy to assemble the small Mn_3O_4 nanoparticles into 3D colloidal spheres;[13a] Very recently, Nakagawa and co-workers produced micrometric linear chains, monolayers, and superstructures (3D arrays) of anisotropic Mn_3O_4 nanocuboids just by changing dispersion media and particle concentration.[23] However, until now, all the reported 3D Mn_3O_4 hierarchical structures are based on 0D (nanoparticles and nanorods) and 1D (nanowire) building blocks, and none of them is composed of 2D building blocks for the hard synthesis of Mn_3O_4 nanosheets and their following self-assembly. Thus, there is strong motivation to develop novel Mn_3O_4 hierarchical structures with 2D building blocks, which

have been widely realized on many other materials such as TiO_2, SnO_2, ZnO and iron oxides.[24]

In this paper, we report a facile and simple process to synthesize 3D hierarchical structures composed of Mn_3O_4 nanosheets at a comparatively low heating temperature and pressure. This new kind of Mn_3O_4 materials were in detail characterized by X-ray diffraction (XRD), scanning electron microscopy (SEM), transmission electron microscopy (TEM), Fourier transforms infrared (FTIR) spectrum and Raman spectrum, respectively. Their application in degradation of organic pollutants in water is also investigated.

Experimental Section

Synthesis of 3D flower-like Mn_3O_4 nanostructures

All of the chemical reagents used in this experiment were analytical grade without further purification. In a typical synthesis of 3D Mn_3O_4 hierarchical structures, manganese sulfate monohydrate (0.19 g) was dissolved in 200 mL distilled water and stirred, then, 1.35 g urea and 1.2 g cetyltrimethylammonium bromide (CTAB) were added under vigorous stirring for 10 min until dissolved completely. Then, the mixed solution was transferred to a 250 mL round-bottomed flask and heated under a constant temperature of 85 ^oC for 24 h. When the solution was cooled to room temperature, 2 g sodium hydroxide (dissolved in 10 mL deionized water) was added to the solution under vigorous stirring, and then 15 mL 30% hydrogen peroxide was dripped into this solution slowly. After the solution was kept immobile for 24 h, the precipitation occurred. The obtained precipitates were filtered and washed several times by deionized water and ethanol, respectively. After drying and grinding, the precipitates were put into muffle furnace for heating at 400 ^oC for 4 h in air with temperature increasing speed at a rate of 10 ^oC/min, and 3D flower-like Mn_3O_4 nanostructures were obtained.

Degradation/Absorption of methylene blue (MB) by Mn_3O_4 in water

The degradation property of the synthesized Mn_3O_4 materials was investigated using MB as standard analog pollutants in water. 20 mg of the as-prepared Mn_3O_4 products were added into a quartz tube which contained 50 mL of 10 mg/L MB dye and 2 mL of 30 wt% H_2O_2. The UV irradiation was carried out on a multi-functional photochemical reaction instrument under 300 W ultraviolet lamp. At given time intervals, 2 mL aliquots of the mixture solution were pipetted out and passed through a polyethersulfone membrane with a pore diameter of 450 nm. The filtrate was gathered and instantly monitored by ultraviolet-visible (UV-Vis) spectroscopy. The degradation rate was calculated by $(A_0\text{-}A)/A_0$, where A_0 was the absorbance at 664 nm at $t=0$ and A was the absorbance at the same wavelength at a given reaction time.

The adsorption experiment of the Mn_3O_4 materials was carried out as follows. 50 mL of 10 mg/L MB dye solution were added by 20 mg of the Mn_3O_4 products, and magnetically stirred at the speed of 600 rpm for 1 hour at room temperature. Then, the mixture was centrifuged at speed of 5000 rpm for 15 min. The upper clear solution was carefully piped out, and the concentration of MB dye is quantified by UV-Vis spectroscopy. The absorption of MB dye on Mn_3O_4 materials can be calculated.

Characterization and Instruments

XRD analysis was carried out on a DLMAX-2200 X-ray diffractometer using Cu Kα radiation (Kα= 1.5406 Å) with an operating voltage of 40 kV and a current of 40 mA. XRD data were recorded with the 2θ ranging from 15 to 70°. Absorption spectra were measured with a Hitachi U-3010 UV-Vis spectrophotometer. FTIR spectra were measured on a Shimadzu FTIR-8400S spectrometer. Raman spectra were recorded using a Renishaw InVia system, with laser excitation at 514.5 nm. SEM images were determined on JSM-6700F instrument at 15 kV. TEM images were performed on a JEOL-200CX instrument, operating at 120 kV. High-resolution transmission electron microscopy (HRTEM) images were obtained in a JEOL-2010 instrument with a point-to-point resolution of 1.94 Å operating at 200 kV. Surface area determination was determined by the Brunauer-Emmett-Teller (BET) approach using an ASAP 2010 surface area analyzer (Micromeritic Instrument Corp.), according to the standard method of N_2 adsorption/desorption. The MB degradation experiments were carried out on a SGY-I multifunctional photochemical reactor with the mercury lamp of 300 W (Nanjing Stonetech Electric Equipment Co. Ltd).

Results and Discussion

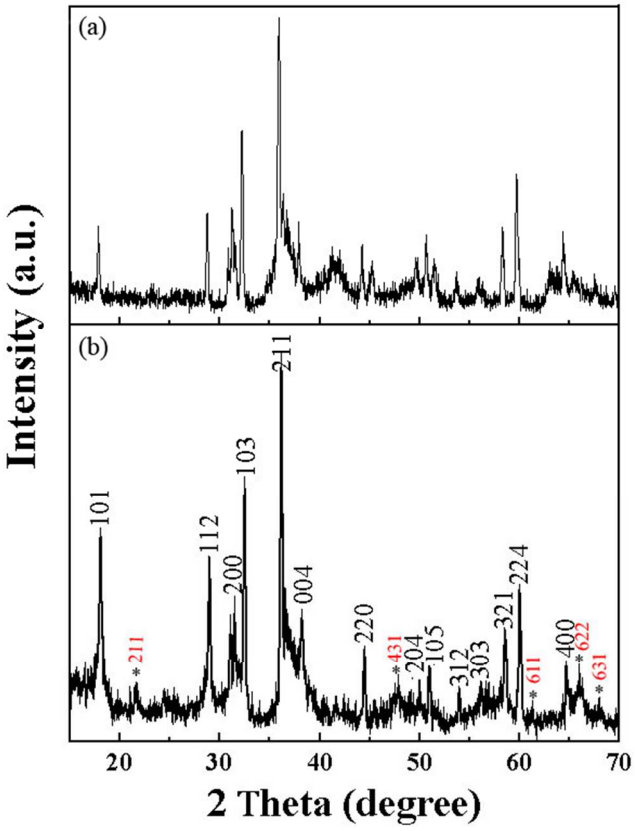

Fig. 1 A typical XRD pattern of 3D flower-like Mn_3O_4 products before (a) and after (b) calcination at 400 ^oC for 4 h . All the diffraction peaks can be perfectly indexed to the tetragonal phase of Mn_3O_4, and the peaks indicated by asterisks correspond to the impurity of Mn_2O_3.

Using the chemical liquid homogeneous precipitation method, the single-crystal 3D flower-like Mn_3O_4 products were prepared. XRD analysis was first carried out to characterize their crystallographic structure. As shown in Fig. 1, all the diffraction peaks of the sample,

either before or after calcination, can be perfectly indexed to the tetragonal phase of Mn_3O_4 (JCPDS Card, No. 80-0382; space group: *I41/amd*; a = 5.780 Å and c = 9.330 Å). This means that the calcination is not the essential step to form crystal phase of Mn_3O_4, but the H_2O_2 oxidation is enough in our preparation process.No characteristic peaks, corresponding to the impurities of MnO_2 or MnOOH etc, are detected. However, there are some Mn_2O_3 ((JCPDS Card No. 41-1442) characteristic peaks appearing in the XRD pattern, which means that there is little Mn_2O_3 impurity in the products.

Then, the morphology and structure of 3D flower-like Mn_3O_4 products were investigated by SEM (Fig. 2a and b). At a low magnification, the as-synthesized materials consist of spherical particles, with sizes ranging from 1 to 5 μm (Fig. 2a). At a high magnification, it is interesting to find that the spherical particles show 3D flower-like structure composed of 2D Mn_3O_4 nanosheets with sizes ranging from hundreds of nanometers to several micrometers (Fig. 2b). In order to further study the microstructure of Mn_3O_4, TEM and high-resolution transmission electron microscopy (HRTEM) were carried out. Fig. 2c is the typical low-magnification TEM image of the 3D Mn_3O_4. It clearly shows that the 3D Mn_3O_4 hierarchical architectures are composed of a certain number of thin-petals with a geometrical shape of nanosheets. These nanosheets grow together with the flower heart as the center and congregate with each other through self-assembly to form the 3D flower-like Mn_3O_4 micro/nanostructures. HRTEM bright-field images clearly supply the internal microstructure information of these 2D Mn_3O_4 nanosheets (Fig. 2d). The clear crystalline lattice fringes demonstrate that these 2D Mn_3O_4 nanosheets are single crystal. The constant value of interplanar spacing between the adiacent atomic lattice fringes is 0.4932 nm, which is consistent with the lattice parameters of the tetragonal structure of the Mn_3O_4 hausmannite phase and corresponds to the {101} plane of tetragonal Mn_3O_4. Furthermore, It should be noted that the 3D flower-like structure of Mn_3O_4 is formed before calcination. As shown in Fig. S1, there is no much difference before and after calcination.

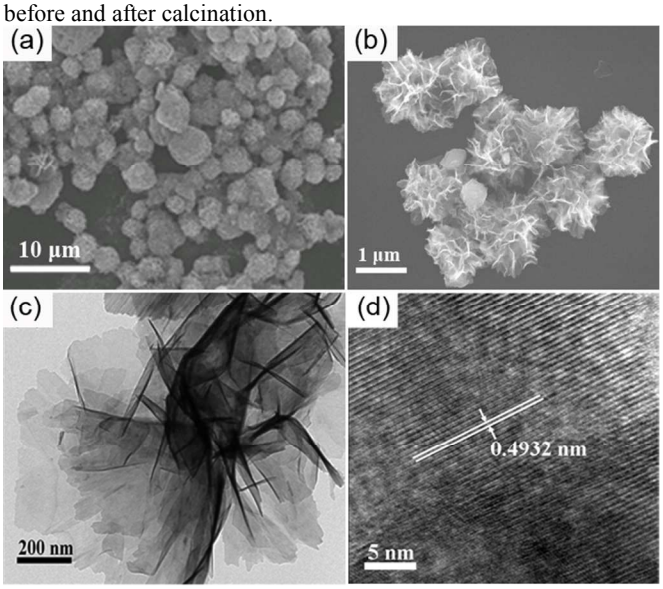

Fig. 2 Typical SEM (a and b) and TEM (c and d) images of the flower-like Mn_3O_4 materials. The lower-magnification images are shown in (a) and (c), while the higher-magnification images are presented in (b) and (d).

The FTIR spectrum further confirms the formation of Mn_3O_4 structure. As shown in Fig. 3a, the spectrum shows similar absorbance with those of Mn_3O_4 obtained in previous studies.[2b] In the region from 650 to 400 cm^{-1}, there are three sharp absorption peaks. The bands around 615 and 513 cm^{-1} can be assigned as the coupling modes between the Mn-O stretching modes, while the band around 429 cm^{-1} can be attributed to the band-stretching mode. The peak centered at 3446 cm^{-1} can owe to the hydroxyl group, which may come from the absorbed water on the surface of Mn_3O_4 products. Fig. 3b is the Raman spectrum of the flower-like Mn_3O_4. A very strong peak at 644 cm^{-1} along with the three weak peaks at 472, 351 and 263 cm^{-1} are consistent with those reported in the literature for Mn_3O_4 rather than Mn_2O_3.[25] The sharp peak at 644 cm^{-1} is assigned to the Mn-O breathing vibration of Mn^{2+} ions, which is found in the mineral hausmannite, as well as in both chemically prepared samples and commercial powders. Thus, based on the results of XRD, TEM, FTIR and Raman spectra, we can confirm that as-synthesized product is composed of single crystal Mn_3O_4 nanosheets and it is interesting that these nanosheets can assemble to 3D Mn_3O_4 spheres with the flower-like morphology.

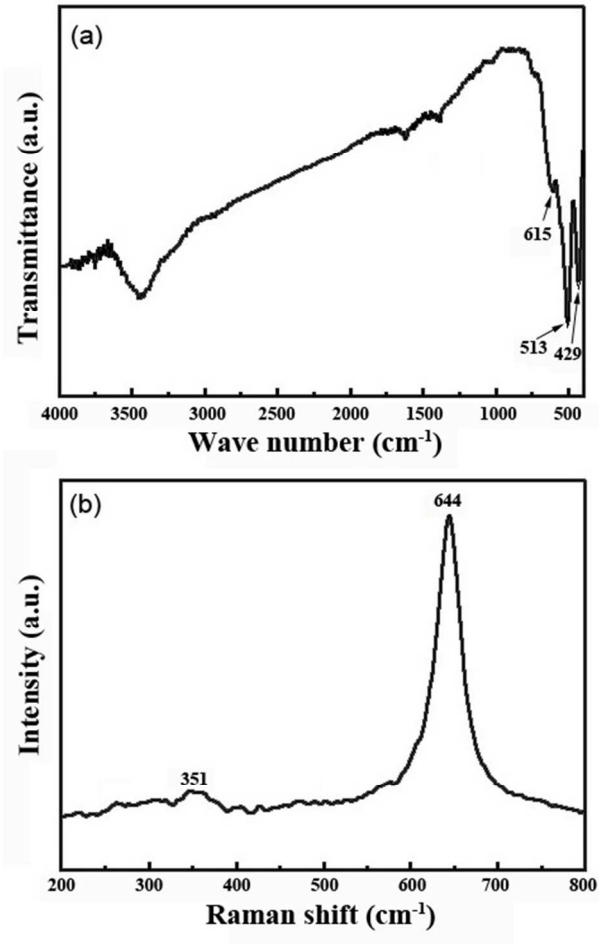

Fig. 3 FTIR (a) and Raman (b) spectra of the flower-like Mn_3O_4 materials

A series of contrast experiments were carried out to investigate the effects of experimental parameters on the morphology and structure of the Mn_3O_4 products. Because the 3D flower-like Mn_3O_4 products were prepared by a hydrothermal reaction, followed bychemical liquid homogeneous precipitation, these two processes were studied separately. First, the effect of the reaction temperature on the hydrothermal reaction was investigated. At a lower temperature (50 ^oC), the flower-like Mn_3O_4 hierarchical structures cannot form, and Mn_3O_4 just shows amorphous morphology (Fig. 4a). When the temperature increases to 70 ^oC, the Mn_3O_4 nanosheets

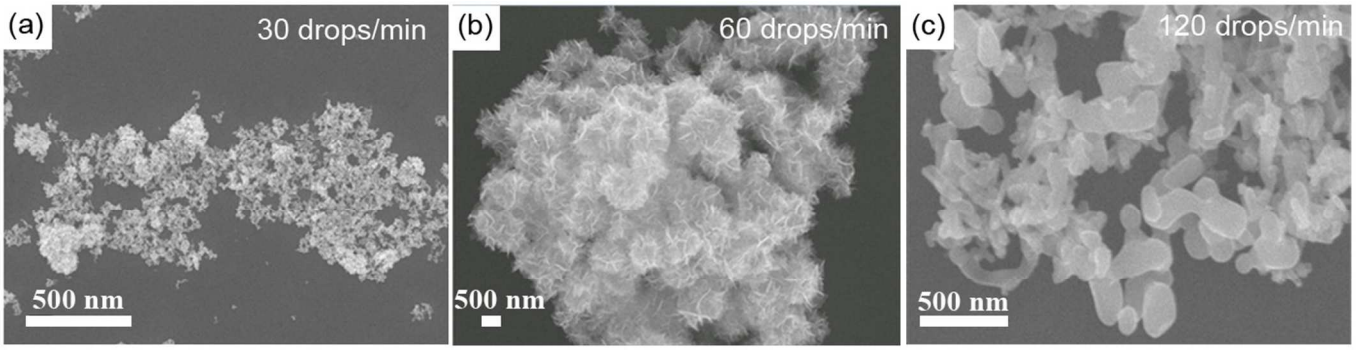

Fig. 5 SEM images of the prepared Mn_3O_4 materials after different speed of NaOH addition. (a): 30 drops/min; (b): 60 drops/min; (c): 120 drops/min.

can be formed, and partly assemble into 3D flower-like hierarchical structures (Fig. 4b). This result indicates that the hydrothermal temperature has important effects on the structure formation of Mn_3O_4 products. Besides the reaction temperature, the reaction time may also play an important role in the formation of 3D flower-like morphology. Fig. 4c is the SEM image of Mn_3O_4 products when the heating time is 12 h at the temperature of 85 ^oC, which clearly shows that the 2D Mn_3O_4 nanosheets have been produced and the initial 3D hierarchical structures are also formed, but until being heated for 24 h, the 3D flower-like hierarchical structures can be well formed (Fig. 4d).

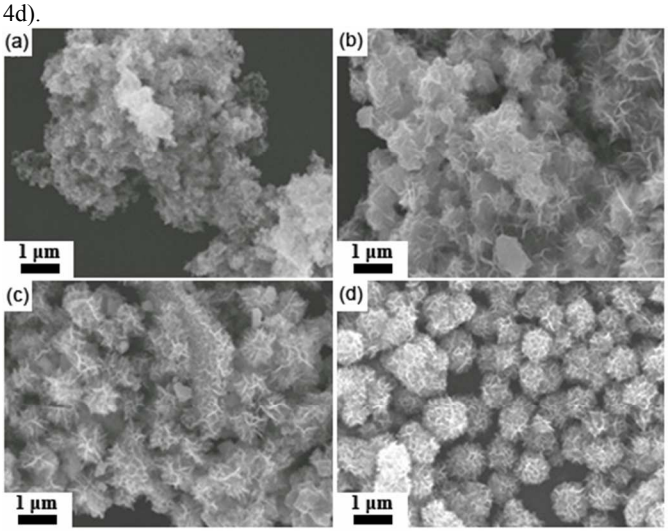

Fig. 4 SEM images of the prepared Mn_3O_4 materials under different hydrothermal reaction conditions. (a): 50 ^oC, 24 h; (b): 70 ^oC, 24 h; (c): 85 ^oC, 12 h; (d): 85 ^oC, 24 h.

As to the process of homogeneous precipitation, it is mainly controlled by the NaOH addition. Since the speed of adding NaOH solutions has been revealed to play a pivotal role in the formation of Mn_3O_4 nanoparticles by our previous experiments,[14a] NaOH addition speed may also have effects on the 3D flower-like structure formation. As shown in Fig. S2, the UV-Vis spectra of the Mn_3O_4 solution with different speed of NaOH addition are similar. There is no characteristic absorption peak of Mn_3O_4 solution. However, the ma morphology Mn_3O_4 is quite different. Fig. 5a is the image of Mn_3O_4 products when the NaOH addition speed is 30 drops per min. The sample consists of ultrafine particles with size of ca 15 nm, and shows serious agglomeration. When the NaOH addition speed increases to 60 drops/min, the obtained Mn_3O_4 sample shows well flower-like spherical morphology (Fig. 5b). However, when the addition speed is up to 120 drops/min, the product displays typical rod-like shapes and smooth surfaces, with the diameter of *ca* 200 nm and length of *ca* 300~500 nm. There are no any ultrafine particles and flower-like spheres observed under the electron microscope (Fig. 5c). Thus, along with the increase of NaOH addition speed, the Mn_3O_4 morphology changes from nanoparticle, then to flower-like microspheres, finally to nanorods. Based on the above experimental results, we considers the NaOH addition speed produced a critical impact in the formation of the 3D flower-like hierarchical structures. However, the exact formation mechanism is not clear yet. We reasonably speculate that the surfactant, CTAB, plays an important role in the Mn_3O_4 formation with different structures. When the NaOH solution is very slowly dripped into the system (about 30 drops/min), CTAB may form a "shell" surrounding the particles and prevents them from growing to larger particles. When the NaOH solution is quickly added (about 120 drops/min), the NaOH significantly disturbs the formation of the "shell" surrounding of the particles; and then Mn_3O_4 nanorods are formed. At a proper speed of adding NaOH, the CTAB could aid Mn_3O_4 to form sheet structure, and then assemble 3D flower-like architecture. The detailed mechanism needs further investigation.

Recently, the organic pollutants are becoming the largest groups of the pollutants in the water environment. Thus, how to eradicate these organic pollutants in the waste water becomes more and more important in the field of sewage treatment.[26] A variety of new technologies have been applied to degrade these organic pollutants, such as physical absorption, chemical coagulation and bio-techniques.[27] However, the former two methods may cause a predictably secondary environmental pollution, and the biological techniques are hard to remove the organic compounds as a result of the high stability of the organic pollutants. Hence, a great number of advanced oxidation processes (AOPs) have been extensively developed to degrade the organic pollutants with the presence of special active catalysts and oxidants.[28] Mn_3O_4 not only shows strong oxidative property, which can oxidize many inorganic and organic compounds, but also is known to be an important and effective catalyst for the degradation of methylene blue,[29] Orange II,[30] phenol,[31] and alizarin yellow R.[32] Several reports have shown that the 3D flower-like hierarchical microstructures were more active than other nanostructured powders (nanoparticles, nanosheets, and nanorods).[33] Therefore, we infered that the as-prepared flower-like Mn_3O_4 materials may be also more efficient than other Mn_3O_4 products in degrading the organic pollutants in water.

The application of flower-like Mn_3O_4 materials used for waste-water treatment was carried out at room temperature. Methylene blue (MB), as a typical industrial pollutant, is chosen as a model to examine the degradation efficiency of organic pollutants by the flower-like Mn_3O_4 materials. From the UV-vis absorption curve of MB, four characteristic peaks were found to be 245, 292, 614 and

664 nm (data not shown), which corresponded to the reported values.[2b] As the degradation of MB proceeds, the characteristic absorption at 664 nm gradually weakens, thus it was chosen for monitoring the MB-degradation process throgh UV/H_2O_2 AOP with the presence of flower-like Mn_3O_4 materials. At the first 10 min, the intensity of the absorption peaks sharply decreased, which means MB was quickly absorbed and degraded. As the reaction proceeds, the drop of the MB absorption peaks continues and finally the solution turns colorless, suggesting MB is heavily degraded. Fig. 6 shows the degradation curve of MB dye solution by different types of Mn_3O_4 materials with the morphology shown in Fig. 5. The degradation rate was calculated by $(A_0\text{-}A)/A_0$, where A_0 was the absorbance at 664 nm at $t=0$ and A was the absorbance at the same wavelength at a given reaction time. It shows that the degree of discoloration is *ca* 49% after UV/H_2O_2 AOP for 3 h by the assistance of Mn_3O_4 nanoparticles, while degradation rate is *ca* 62% by Mn_3O_4 nanorods. However, as to the flower-like Mn_3O_4, the degradation efficiency of MB is up to *ca* 73% after the same process. The degradation efficiency increases significantly from the Mn_3O_4 nanoparticles, nanorods to flower-like hierarchical structures. This is similar with that of flower-like ZnO hierarchical architectures, showing the highest efficiency in the photodegradation of rhodamine B compared with the monomorphological ZnO powders of nanoparticles, nanosheets, and nanorods.[33] The high degradation efficiency of flower-like Mn_3O_4 may come from that the net-like arrangement of nanosheets in the 3D structures would effectively prevent aggregation and thus maintain a large active surface area.[33]

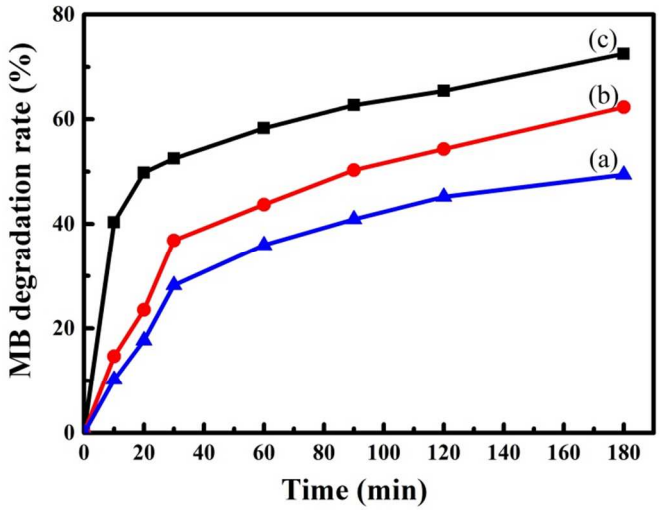

Fig. 6 Time profiles of MB degradation by the UV/H_2O_2 AOP at room temperature, with the presence of different types of Mn_3O_4 materials: a) Mn_3O_4 nanoparticles with the morphology shown in Fig. 5(a), b) Mn_3O_4 nanoparticles with the morphology shown in Fig. 5(c), c) flower-like Mn_3O_4 hierarchical structures with the morphology shown in Fig. 5(b).

In order to elucidate the relationship between the structure and performance Mn_3O_4, the specific surface area and porosity were measured by the N_2 adsorption-desorption method (or called Brunauer-Emmett-Teller method, BET). The inset image of Fig. 7 shows the BET surface area of the three kinds of Mn_3O_4 materials, calculated to be 108, 126, and 156 m^2/g for nanoparticles, nanorods, and 3D flower-like nanostructure, respectively. Fig. 7 is the adsorption-desorption isotherms of the 3D flower-like Mn_3O_4 nanostructures, exhibiting type IV mode, which is related to mesoporous materials. The pore size distribution is estimated using the BJH model, indicating a broad peak from 10 nm to 100 nm, which means the pores in the 3D flower-like Mn_3O_4 nanostructures are not uniform (Fig. 7). There is on distinct pore size distribution in the Mn_3O_4 nanoparticles and nanorods. In general, the surface area is one of the most crucial parameter to understand the behaviour of a material, because the material reacts with its surroundings via its surface, and a higher surface area material is more likely to adsorb more molecules, and react faster than a similar material with a lower surface area. The different BET surface areas of the three kinds of Mn_3O_4 nanomaterials may imply that they have different reaction initial rates and catalytic activities, and the order would be 3D flower-like nanostructures, nanorods and nanoparticles. This result is similar with our published paper, which indicates the Mn_3O_4 nanofractals, with the highest BET surface area, have the highest catalytic activity, compared with other two kinds of Mn_3O_4 particles.[14a] Furthermore, the MB adsorption experiment of the three kinds of Mn_3O_4 materials was also carried out. The result shows the absorption of MB dye on nanoparticles, nanorods, and 3D flower-like nanostructures is 5.6, 7.1, and 9.2 μg/mg, respectively. This may again explain why 3D flower-like Mn_3O_4 nanostructures have the highest initial reaction rate.

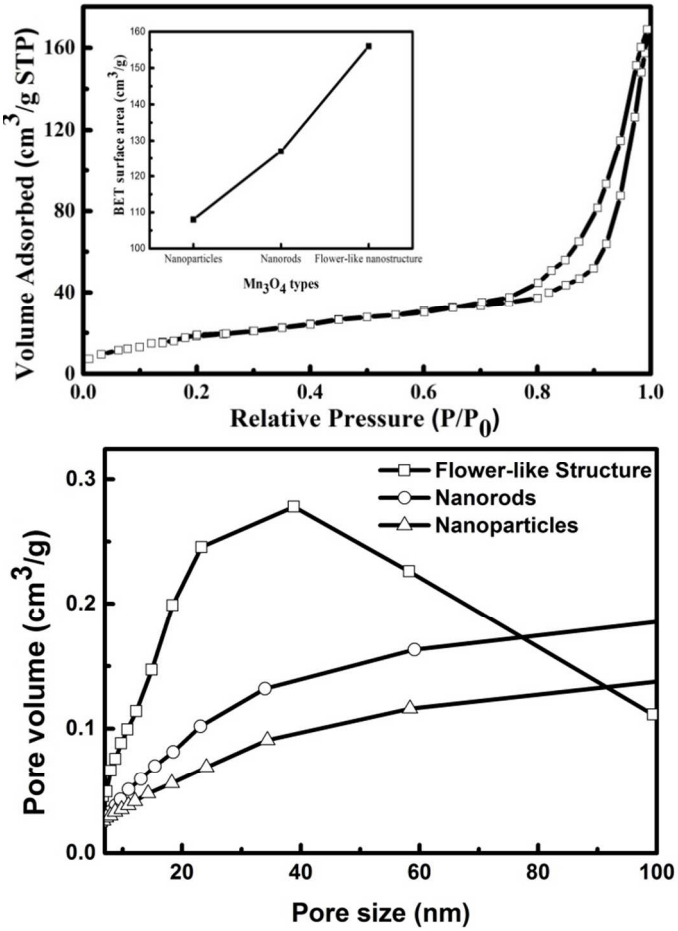

Fig. 7 Nitrogen adsorption-desorption isotherms of 3D flower-like Mn_3O_4 nanostructure (up) and pore size distribution curve of three kinds of Mn_3O_4 nanostructures (down). Inset: the BET surface area of Mn_3O_4 with the morphology of and nanoparticle, nanorod and 3D flower-like nanostructure.

Then, to clarify the MB degradation is from the photocatatic property of the flower-like Mn_3O_4 materials, several control experiments were carried out and results are shown in Fig. 8. When only H_2O_2 is added into MB solution, the MB degradation rate is little, only about 8% without UV irradiation and 13% under UV

irradiation. However，when Mn_3O_4 and H_2O_2 are added to the MB solution, the degradation rate can increase to 40% without UV irradiation after 3 h mixture. Then, after both Mn_3O_4 and H_2O_2 are added and the experiment is carried out under UV irradiation, the obvious discoloration occurrs. After 3 h exposure, the MB degradation rate is up to 73%, evidently higher than that of 40% without UV irradiation. Therefore, the MB degradation efficiency of the flower-like Mn_3O_4 materials can be significantly enhanced by UV irradiation, which means that the MB degradation process is more effective for the photocatalic property of Mn_3O_4.

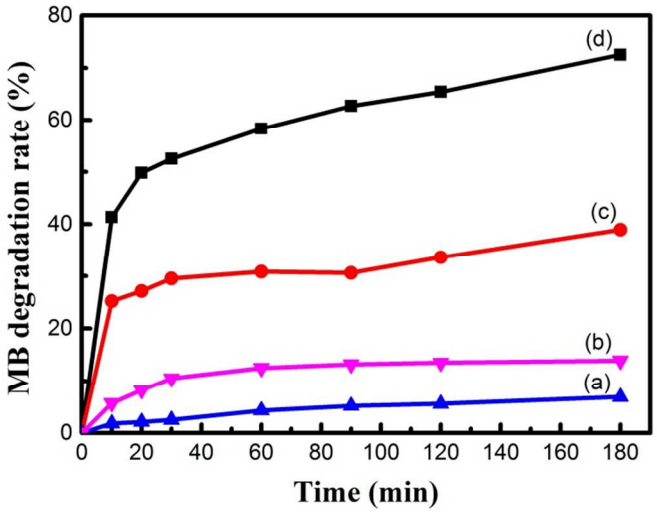

Fig. 8 Time profiles of MB degradation by flower-like Mn_3O_4 materials at room temperature: a) H_2O_2 and MB; b) H_2O_2 and MB and UV irradiation; c) H_2O_2, Mn_3O_4 and MB; d) H_2O_2, Mn_3O_4, MB and UV irradiation.

Although it is evidence that the flower-like Mn_3O_4 materials can the most remarkably photocatalyze the dye degradation, compared with the countparts with the morphology of nanoparticle and nanorod. However, the recycle photocatalytic performance is not good. The MB dye degradation rate in three cycles was 75.6%, 52.3%, and 34.7%, after 180 min of reaction, respectively. The result reveals the catalytic efficiency of the catalyst has a much decrease after each cycle. The reason may be partly due to inescapable reduction of Mn_3O_4 by MB dyes and lacking some of its adsorption ability.[34]

Conclusions

In summary, 3D flower-like Mn_3O_4 hierarchical structures were successfully prepared by a facile and simple process at a comparatively low heating temperature and pressure. This process involves a hydrothermal reaction and a chemical liquid homogeneous precipitation. These flower-like Mn_3O_4 materials are composed of Mn_3O_4 nanosheets with sizes ranging from hundreds of nanometers to several micrometers. The control experiments indicate that the hydrothermal temperature and NaOH addition speed have the critical effects on the formation of 3D flower-like morphology. Compared with the countparts with the morphology of nanoparticle and nanorod, the flower-like Mn_3O_4 materials can remarkably photocatalyze the dye degradation during UV/H_2O_2 AOP, which comes from their high BET surface area and good absorption ability.

Acknowledgements

We are grateful to Prof. Zhiwen Chen for his kind help. This work was financially supported by the National Natural Science Foundation of China (11025526, 21371118), the China 973 project (2011CB933402), Program for Changjiang Scholars and Innovative Research Team in University (IRT13078), Shanghai Science and Technology Committee (13R1414900) and Shanghai Municipal Education Commission (12YZ015).

Notes and references

[a] Shanghai Applied Radiation Institute, School of Environmental and Chemical Engineering, Shanghai University, Shanghai 200444, P. R. China; E-mail: mhwu@shu.edu.cn

[b] Institute of Nanochemistry and Nanobiology, Shanghai University, Shanghai 200444, P. R. China; E-mail: xydeng@shu.edu.cn

1 a) J. Gao, M. A. Lowe and H. D. Abruna, *Chem. Mater.* 2011, **23**, 3223-3227; b) T. Yu, J. Moon, J. Park, Y. I. Park, H. Bin Na, B. H. Kim, I. C. Song, W. K. Moon and T. Hyeon, *Chem. Mater.* 2009, **21**, 2272-2279; c) H. L. Wang, L. F. Cui, Y. A. Yang, H. S. Casalongue, J. T. Robinson, Y. Y. Liang, Y. Cui and H. J. Dai, *J. Am. Chem. Soc.* 2010, **132**, 13978-13980.

2 a) J. J. Li, L. Li, F. Wu, L. Zhang and X. M. Liu, *Catal. Commun.* 2013, **31**, 52-56; b) Z. C. Bai, B. Sun, N. Fan, Z. C. Ju, M. H. Li, L. Q. Xu and Y. T. Qian, *Chem. Eur. J.* 2012, **18**, 5319-5324; c) Z. Y. Fei, B. Sun, L. Zhao, W. J. Ji and C. T. Au, *Chem. Eur. J* 2013, **19**, 6480-6487; d) J. W. Xiao, L. Wan, X. Wang, Q. Kuang, S. Dong, F. Xiao and S. Wang, *J. Mater. Chem. A* 2014, **2**, 3794-3800; e) P. Q. Zhang, Y. G. Zhan, B. X. Cai, C. C. Hao, J. Wang, C. X. Liu, Z. J. Meng, Z. L. Yin and Q. Y. Chen, *Nano Res.* 2010, **3**, 235-243.

3 a) Z. C. Bai, N. Fan, Z. C. Ju, C. L. Guo, Y. T. Qian, B. Tang and S. L. Xiong, *J. Mater. Chem. A* 2013, **1**, 10985-10990; b) S. Luo, H. C. Wu, Y. Wu, K. L. Jiang, J. P. Wang and S. S. Fan, *J. Power Sources* 2014, **249**, 463-469.

4 a) W. S. Seo, H. H. Jo, K. Lee, B. Kim, S. J. Oh and J. T. Park, *Angew. Chem. Int. Ed.* 2004, **43**, 1115-1117; b) L. Z. Ren, S. X. Wu, M. Yang, W. Q. Zhou and S. W. Li, *J. Appl. Phys.* 2013, **114**; c) N. N. Zhao, W. Nie, X. B. Liu, S. Z. Tian, Y. Zhang and X. L. Ji, *Small* 2008, **4**, 77-81.

5 a) L. Armelao, D. Barreca, G. Bottaro, A. Gasparotto, S. Gross, C. Maragno and E. Tondello, *Coordin. Chem. Rev.* 2006, **250**, 1294-1314; b) Y. Li and W. J. Shen, *Chem. Soc. Rev.* 2014, **43**, 1543-1574; c) N. R. Shiju and V. V. Guliants, *Appl. Catal. A Gen.* 2009, **356**, 1-17; d) A. K. Viswanath, *J. Nanosci. Nanotechnol.* 2014, **14**, 1253-1281.

6 a) X. Wang and Y. Li, *J. Am. Chem. Soc.* 2002, **124**, 2880-2881; b) T.-Z. Ren, Z.-Y. Yuan, W. Hu and X. Zou, *Micropor. Mesopor. Mater.* 2008, **112**, 467-473; c) Y. Li, H. Tan, X.-Y. Yang, B. Goris, J. Verbeeck, S. Bals, P. Colson, R. Cloots, G. Van Tendeloo and B.-L. Su, *Small* 2011, **7**, 475-483.

7 N. Wang, L. Guo, L. He, X. Cao, C. Chen, R. Wang and S. Yang, *Small* 2007, **3**, 606-610.

8 a) T. Ould-Ely, D. Prieto-Centurion, A. Kumar, W. Guo, W. V. Knowles, S. Asokan, M. S. Wong, I. Rusakova, A. Lüttge and K. H. Whitmire, *Chem. Mat.* 2006, **18**, 1821-1829; b) W. S. Seo, H. H. Jo, K. Lee, B. Kim, S. J. Oh and J. T. Park, *Angew. Chem. Int. Ed.* 2004, **43**, 1115-1117; c) I. Rusakova, T. Ould-Ely, C. Hofmann, D. Prieto-Centurión, C. S. Levin, N. J. Halas, A. Lüttge and K. H. Whitmire, *Chem. Mat.* 2007, **19**, 1369-1375.

9 N. Zhao, W. Nie, X. Liu, S. Tian, Y. Zhang and X. Ji, *Small* 2008, **4**, 77-81.

10 W. Wang, C. Xu, G. Wang, Y. Liu and C. Zheng, *Adv. Mater.* 2002, **14**, 837-840.

11 a) Y. W. Tan, L. R. Meng, Q. Peng and Y. D. Li, *Chem. Commun.* 2011, *47*, 1172-1174; b) W. Z. Wang and L. Ao, *Cryst. Growth Des.* 2008, **8**, 358-362.

12 Z. Bai, N. Fan, Z. Ju, C. Guo, Y. Qian, B. Tang and S. Xiong, *J. Mater. Chem. A* 2013, **1**, 10985-10990.
13 a) P. Li, C. Nan, Z. Wei, J. Lu, Q. Peng and Y. Li, *Chem. Mater.* 2010, **22**, 4232-4236. b) S. K. Bikkarolla, F. Yu, W. Zhou, P. Joseph,, P. Cumpson and P. Papakonstantinou, *J. Mater. Chem. A* 2014, **2**, 14493-14501; c) P. Si, X.-C. Dong, P. Chen and D.-H. Kim, *J. Mater. Chem. B* 2013, **1**, 110-115.
14 a) C. Chen, G. Ding, D. Zhang, Z. Jiao, M. Wu, C. H. Shek, C. M. Wu, J. K. Lai and Z. Chen, *Nanoscale* 2012, **4**, 2590-2596; b) Z. Chen, Z. Jiao, D. Pan, Z. Li, M. Wu, C. H. Shek, C. M. Wu and J. K. Lai, *Chem. Rev.* 2012, **112**, 3833-3855.
15 H. Huang, Q. Yu, X. Peng and Z. Ye, *Chem. Commun.* 2011, **47**, 12831-12833.
16 L. Yi and G. Hu, *RSC Adv.* 2013, **3**, 23461-23469.
17 C. Chen, H. Jian, X. Fu, Z. Ren, M. Yan, G. Qian and Z. Wang, *RSC Adv.* 2014, **4**, 5367-5370.
18 a) K. Ariga, Q. Ji, M. J. McShane, Y. M. Lvov, A. Vinu and J. P. Hill, *Chem. Mater.* 2011, **24**, 728-737; b) Z. Sun, T. Liao, K. Liu, L. Jiang, J. H. Kim and S. X. Dou, *Nano Res.* 2013, **6**, 726-735.; c) J. Cheng, R. Che, C. Liang, J. Liu, M. Wang and J. Xu, *Nano Res.* 2014, **7**, 1043-1053.; d) S. Li, A. Li, R. Zhang, Y. He, Y. Zhai and L. Xu, *Nano Res.* 2014, **7**, 1116-1127.
19 J. Gong, G. Li and Z. Tang, *Nano Today* 2012, **7**, 564-585.
20 G. J. Soler-Illia and O. Azzaroni, *Chem. Soc. Rev.* 2011, **40**, 1107-1150.
21 J. Kao, K. Thorkelsson, P. Bai, B. J. Rancatore and T. Xu, *Chem. Soc. Rev.* 2013, **42**, 2654-2678.
22 a) Z. C. Wu, K. Yu, Y. B. Huang, C. Pan and Y. Xie, *Chem. Cent. J.* 2007, **1**, 8; b) C. Du, J. Yun, R. K. Dumas, X. Yuan, K. Liu, N. D. Browning and N. Pan, *Acta Mater.* 2008, **56**, 3516-3522.
23 Y. Nakagawa, H. Kageyama, Y. Oaki and H. Imai, *J. Am. Chem. Soc.* 2014, **136**, 3716-3719.
24 H. K. Wang and A. L. Rogach, *Chem. Mater.* 2014, **26**, 123-133.
25 R. Bussamara, W. W. Melo, J. D. Scholten, P. Migowski, G. Marin, M. J. Zapata, G. Machado, S. R. Teixeira, M. A. Novak and J. Dupont, *Dalton. Trans.* 2013, **42**, 14473-14479.
26 O. Zuloaga, P. Navarro, E. Bizkarguenaga, A. Iparraguirre, A. Vallejo, M. Olivares and A. Prieto, *Anal. Chim. Acta* 2012, **736**, 7-29.
27 M. Klavarioti, D. Mantzavinos and D. Kassinos, *Environ. Int.* 2009, **35**, 402-417.
28 A. Di Paola, E. García-López, G. Marcì and L. Palmisano, *J.Hazardous Mat.* 2012, **211–212**, 3-29.
29 a) J.-H. Park, I. Jang, Y. Kang, Y. C. Kim and S.-G. Oh, *Colloid. Surf. A* 2014, **441**, 340-345; b) J.-H. Park, I. Jang, B. Kwon, S.-C. Jang and S.-G. Oh, *Mater. Res. Bull.* 2013, **48**, 469-475; c) L. Zhang, Y. Nie, C. Hu and X. Hu, *J. Hazardous Mat.* 2011, **190**, 780-785; d) X. Peng and I. Ichinose, *Nanotechnology* 2011, **22**, 015701; e) T. Rhadfi, J.-Y. Piquemal, L. Sicard, F. Herbst, E. Briot, M. Benedetti and A. Atlamsani, *Appl. Catal. A Gen.* 2010, **386**, 132-139.
30 Y. Yao, C. Xu, S. Yu, D. Zhang and S. Wang, *Ind. Eng. Chem. Res.* 2013, **52**, 3637-3645.
31 a) E. Saputra, S. Muhammad, H. Sun, H.-M. Ang, M. O. Tadé and S. Wang, *J. Colloid Interf. Sci.* 2013, **407**, 467-473; b) E. Saputra, S. Muhammad, H. Sun, H.-M. Ang, M. O. Tadé and S. Wang, *Appl. Catal. B Environ.* 2013, **142–143**, 729-735.
32 K. A. M. Ahmed, H. Peng, K. Wu and K. Huang, *Chem. Eng. J.* 2011, **172**, 531-539.
33 C. Pan, L. Dong, B. Qu and J. Wang, *J. Nanosci. Nanotechnol.* 2011, **11**, 5042-5048.
34 X. Hao, J. Zhao, Y. Zhao, D. Ma, Y. Lu, J. Guo and Q. Zeng, *Chem. Eng. J.* 2013, **229**, 134-143.

Table of Content

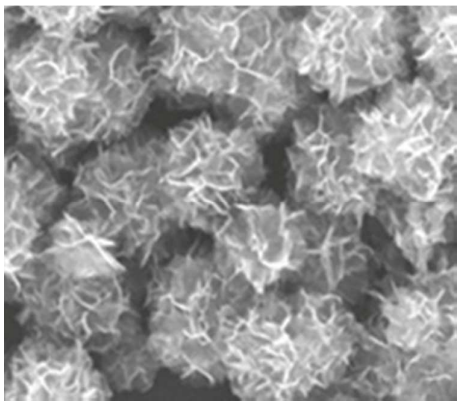

The 3D hierarchical structures composed of Mn3O4 nanosheets are synthesized and show high photocatalysis performance.